HHS Public Access

Author manuscript

Nat Cell Biol. Author manuscript; available in PMC 2012 November 01.

Published in final edited form as:

Nat Cell Biol. ; 14(5): 488–501. doi:10.1038/ncb2473.

Distinct and separable activities of the endocytic clathrin coat components Fcho1/2 and AP-2 in developmental patterning

P. K. Umasankar[1], **Subramaniam Sanker**[1], **James R. Thieman**[1], **Souvik Chakraborty**[1], **Beverly Wendland**[2], **Michael Tsang**[3], and **Linton M. Traub**[1,4]

[1]Department of Cell Biology, University of Pittsburgh School of Medicine, Pittsburgh, PA 15261 USA

[2]Department of Biology, The Johns Hopkins University, Baltimore, MD 21218 USA

[3]Department of Developmental Biology, University of Pittsburgh School of Medicine, Pittsburgh, PA 15213 USA

Abstract

Clathrin-mediated endocytosis occurs at multiple independent import sites on the plasma membrane, but how these positions are selected and how different cargo is simultaneously recognized is obscure. FCHO1 and FCHO2 are early-arriving proteins at surface clathrin assemblies and are speculated to act as compulsory coat nucleators, preceding the core clathrin adaptor AP-2. Here, we show the μ-homology domain (μHD) of FCHO1/2 represents a novel endocytic interaction hub. Translational silencing of *fcho1* in zebrafish embryos causes strong dorsoventral patterning defects analogous to Bmp signal failure. The Fcho1 μHD interacts with the Bmp receptor Alk8, uncovering a new endocytic component that positively modulates Bmp signal transmission. Still, the *fcho1* morphant phenotype is distinct from severe embryonic defects apparent when AP-2 is depleted. Our data thus contradict the primacy of FCHO1/2 in coat initiation.

INTRODUCTION

Clathrin-mediated endocytosis is a major mechanism for the selective internalization of cell surface components and extracellular macromolecules[1,2]. The import sites contain clathrin triskelia assembled into a polygonal lattice[3]. As the lattice curves by incorporating pentagonal facets and projects into the cell interior, select cargo is packaged into the clathrin-coated invagination. Preferential retention of cargo within the bud depends on cytosol-oriented sorting signals[4-6]. A heterotetrameric AP-2 adaptor complex and numerous

[4]To whom correspondence should be addressed at: Department of Cell Biology University of Pittsburgh School of Medicine 3500 Terrace Street, S311 BST Pittsburgh, PA 15261 Tel: (412) 648-9711 Fax: (412) 648-9095 traub@pitt.edu.

Contributions P.K.U., S.S., J.R.T., S.C., L.M.T. designed, performed and interpreted various experiments. B.W. and M.T. provided intellectual input, contributed to experimental design and advised on data interpretation. L.M.T. conceived and directed the overall project and wrote the manuscript with comments from all the authors.

Competing financial interests The authors declare no competing financial interests.

clathrin-associated sorting proteins (CLASPs) identify structurally disparate sorting signals[6]; this recognition allows non-competitive grouping of dissimilar cargo into single clathrin-coated buds. The processes of coat assembly, cargo capture and budding takes less than a minute, and eukaryotic cells have hundreds of spatially-discrete clathrin-coated structures forming on the surface[3]. Precisely how buds initiate at defined locations is unclear[7,8]. Certainly, phosphatidylinositol 4,5-bisphosphate (PtdIns(4,5)P_2) is pivotal since depleting this lipid triggers swift dissolution of surface coats[9,10]. Because AP-2 and numerous CLASPs and clathrin accessory proteins bind physically to PtdIns(4,5)P_2, current models invoke stochastic but simultaneous encounters of these molecules with PtdIns(4,5)P_2, themselves, cargo and clathrin to begin coat polymerization on a patch of membrane[6,11]. Recently, however, on the basis of two PtdIns(4,5)P_2-binding proteins invariantly preceding the arrival of AP-2 and clathrin at nascent bud sites, FCH domain only 1 (FCHO1) and FCHO2 were proposed to be functionally redundant pioneer proteins demarcating sites of future clathrin assembly[12].

Here, we examine the endocytic activity of the modular FCHO1 and FCHO2 proteins to address the following questions: What molecular interactions distinguish the various protein domains? What role do Fcho1 and Fcho2 play in zebrafish embryonic development? Are Fcho1 and Fcho2 functionally interchangeable? And, if FCHO1/2 is obligatory for clathrin-coat nucleation, does the phenotype of Fcho1+2-compromised embryos parallel that of AP-2 morphants? We find Fcho1 operates during dorsoventral (DV) patterning of the embryo and associates with activin receptor-like kinase 8 (Alk8/*lost-a-fin*), a type I BMP receptor involved in signaling ventral cell fates[13,14]. Yet AP-2 depletion causes a much more penetrant, broadly severe and earlier developmental phenotype, indicating AP-2 function is not dependent on Fcho1/2.

RESULTS

FCHO1 and FCHO2 are members of the muniscin subfamily of EFC domain proteins evolutionarily conserved from unicellular eukaryotes to mammals[15,16]. These paralogues play a functionally redundant role beginning at the earliest assembly stages of clathrin-mediated endocytosis[7,12,15,17,18]. HeLa cells express transcripts for both FCHO1 and FCHO2 but endogenous FCHO1 protein is undetectable with antibodies[19]. Transient expression of GFP-tagged FCHO1 reveals scattered bright puncta on the ventral surface, but a diffuse membrane-tethered population becomes evident with higher over-expression (Fig. S1a). The heterogeneously sized fluorescent structures in cells expressing low-level GFP-FCHO1 colocalize with AP-2 but are spatially distinct from peripheral APPL1-positive endosomes or more centrally positioned EEA1-positive endosomes (Fig. S1b-e)[20]. More abundant endogenous FCHO2 populates similar punctate structures to GFP-FCHO1 at steady state with considerable (~75%) overlap, although not perfect coincidence, with AP-2 (Fig. S1f-i). These findings confirm FCHO1/2 operate at clathrin-coated structures at the cell surface.

The FCHO endocytic hub

FCHO1 and FCHO2 are modular proteins (Fig. S1j). The N-terminal EFC domain is connected to a ~280 residue C-terminal μHD by a linker of differing length in the paralogues. The first 270 residues of human FCHO1 and FCHO2, encoding a helical EFC domain monomer[21], are 58% identical. Accordingly, dose-dependent association of purified FCHO1 EFC domain with PtdIns(4,5)P_2-containing liposomes parallels that of the FCHO2 (Fig. S1k)[12,21]. Binding to liposomes lacking PtdIns(4,5)P_2 is ~10-fold less efficient. The membrane binding and curvature sensing/inducing properties[21] of the antiparallel EFC domain dimer in FCHO1 and FCHO2 are thus similar.

The linker region—Protein disorder predictions indicate the EFC- and μHD-separating residues (300-600) of FCHO1 comprise a low-complexity, largely unstructured segment. Intrinsic disorder is a hallmark of numerous endocytic factors that bind AP-2 utilizing short, tandemly-arrayed peptide motifs in the flexible region[5,8,22]. GST-fusion proteins encompassing the central portion of FCHO1 engage AP-2 in pull-down assays (Fig. 1a, b). The apparent affinity of this association with AP-2 is weaker than the C-terminal segment of ARH, which engages AP-2 with a K_D of ~1 μM[23,24]. The major AP-2 interaction determinant(s) in FCHO1 is between residues 267-442 (Fig. 1a, b). Unlike ARH, the central segment of FCHO1 does not bind clathrin directly (Fig. 1b). FCHO2 does not associate with AP-2 (Fig. S2a); the shorter central linker in FCHO2 displays <30% identity with FCHO1, probably explaining the absence of an AP-2 interaction motif(s).

FCHO1 binds AP-2 through the globular appendage domain of the large α subunit, but some association with the β2-subunit appendage is also evident (Fig. 1c). The contact site upon the α appendage is the platform subdomain since a W840A substitution abolishes binding (Fig. 1d); a sandwich subdomain disruption (Q782A)[25,26] has no effect on binding. Yet RNAi suppression of AP-2, causing pronounced accumulation of dispersed transferrin receptors at the cell surface[27,28], is still compatible with surface-clustered FCHO1 or -2 puncta (Fig. 1e-l) also containing clathrin (Fig. 1m) and eps15 (Fig. S2b), in line with these proteins being constituents of a pioneer unit[7,12,17]. AP-2 depletion is seen on immunoblots (Fig. 1n). Thus, despite binding AP-2, the heterotetramer is not necessary for FCHO1 (or FCHO2) surface puncta. This is consistent with FCHO2 not contacting AP-2 directly and also supported by truncation analysis; while full-length GFP-FCHO1 (1-889) masses at AP-2 patches, GFP-FCHO1 (1-275) and (1-609) are diffusely plasma membrane associated (Fig. 1o-q) while GFP-FCHO1 (265-467) and (265-609) are cytosolic (Fig. S2). By contrast, GFP-μHD (609-889) populates clathrin spots, albeit not as efficiently as the full-length protein (Fig. 1r). Precise deposition of FCHO1 at clathrin foci therefore depends, in part, on the C-terminal μHD.

The μHD—Muniscins associate with eps15[12,15,29]. Reciprocal pull-down assays using a GST fusion with the C-terminus of eps15 (595-896) confirm binding requires the μHD (Fig. 2a). μHDs also associate with intersectin 1 (Fig. 2b), another EH (and SH3) domain scaffold protein involved in clathrin-mediated endocytosis[30,31] that heterooligomerizes with eps15[32]. Yet, unlike the AP-2 α-subunit appendage, which also binds eps15 and intersectin to a similar extent, the μHDs do not interact with endocytic factors like AP180, amphiphysin or

epsin 1. The capacity of FCHO1/2 to associate with membranes in a PtdIns(4,5)P_2-dependent manner and engage AP-2 and other core endocytic components (eps15, intersectin) distinguishes these proteins as dedicated endocytic factors. This is consistent with positioning of FCHO1/2 at clathrin structures on the plasma membrane (Fig. 1).

The FCHO1/2 μHDs also associate with eps15, eps15R, and intersectin in HeLa lysates. In addition, Dab2, Hrb and CALM, three tandem Asn-Pro-Phe-containing CLASPs bind the μHDs in a concentration-dependent manner (Fig. 2c). Three observations rule out that these associations are indirect and mediated by Asn-Pro-Phe sequences binding to the EH domain scaffolds (eps15/R and intersectin). First, Dab2, Hrb and CALM binding does not parallel binding of the EH domain proteins to GST-μHDs. Second, Hrb and CALM bind efficiently to only the FCHO1 μHD and neither FCHO2 nor SGIP1, despite all exhibiting robust eps15 and intersectin interactions. Third, preincubating HeLa lysates with GST-FCHO2 μHD removes the majority of eps15 and intersectin, but remaining Hrb and CALM engage GST-FCHO1 μHD in second-stage incubations indistinguishably from GST-preincubated lysate (Fig. 2d). This reveals that association of Dab2, Hrb and CALM with the FCHO1 μHD is independent of EH domain proteins and highlights a functional difference between FCHO1 and FCHO2/SGIP1 μHDs.

The Asp-Pro-Phe tripeptide-rich C terminus of eps15 was used to delineate the FCHO1 μHD-binding region (Fig. 2e, f). A limited tract positioned between eps15 residues ~600 and 660 is recognized by the μHD. Since this short eps15 (595-660) peptide efficiently competes with cytosolic Hrb, CALM and Dab2 in assays at lower concentrations than required to displace eps15R, intersectin or eps15 (Fig. 2g), all likely engage the FCHO1 μHD through a common or partly overlapping interaction surface, but with the scaffolds binding with higher apparent affinity. Numerous important accessory proteins and CLASPs thus converge on the FCHO1 μHD (Fig. 2h) and, therefore, like the AP-2 appendage domains[6,8], this domain represents a novel endocytic hub.

FCHO1 affects embryogenesis

Misexpression of mammalian FCHO1 in zebrafish confirms the μHD importance. On microinjecting synthetic GFP-FCHO1 (1-889) mRNA into 1-cell stage embryos, fluorescence is visible during the early gastrula period, ~5 hours post fertilization (hpf) (Fig. 3a). Coinjection of a membrane-tethered RFP marker shows GFP-FCHO1 concentrates at the blastomere plasma membrane, but in discontinuous puncta as opposed to the uninterrupted RFP. The punctate GFP-FCHO1 pattern overlaps with endogenous AP-2 (Fig. 3b, c). By 24 hpf, microinjected ectopic mammalian FCHO1 produces a gain-of-function phenotype. Unlike controls, the FCHO1-expressing embryos are cyclopic and mildly ventralized, with small head regions, misshapen trunk somites, and loss of notochord tissue in severely affected embryos (Fig. 3d-j). Comparative *in situ* localization of transcripts for dorsally specified axial mesoderm, *no-tail* and *sonic hedgehog*, confirms disruption of dorsal patterning. Strikingly, misexpression of similar amounts of a μHD-truncated FCHO1 (1-609; ΔμHD) mRNA leads to strong dorsalization (Fig. 3k). Embryos now show posteriorly shortened and twisted body axes, loss of the yolk extension and tail. The most severe resemble C4/C5 category *snailhouse* (*bmp7*) and *swirl* (*bmp2b*) mutant embryos[33,34].

Injection of FCHO1 μHD (609-889) mRNA alone phenocopies FCHO1 (1-609) overexpression (Fig. 3j, l) indicating that the dominant-negative effect derives from uncoupling the linked domains and that the normal operation of FCHO1 requires physical connection of the EFC and μHD regions. These reciprocal dysmorphic effects suggest muniscins participate in early embryogenesis. In fact, because DV patterning is governed in part by Bmp signaling[35], Fcho1 may assist operation of Bmp receptors during gastrulation. The Smad1/5/8 transcription factors are direct phosphotargets of the type I Bmp receptor Alk8[36], and phosphoSmad (pSmad1/5/8) localization is grossly misplaced dorsally in constitutively-active (CA*) *alk8* mRNA-injected embryos (Fig. 3m, n). Likewise, ectopic FCHO1 expression drives notable, but weaker, dorsal expansion of nuclear pSmad1/5/8 localization in gastrulas (Fig. 3o-s), indicating hyperactive Bmp signaling.

D. rerio Fcho1 and Fcho2 in DV patterning

A single gene encodes Fcho1 (LOC565812) and Fcho2 (ZDB-GENE-050522-228) in zebrafish. The structural and topological features are conserved in the teleost proteins (Fig. S3) and maternally deposited transcripts for both Fcho1 and Fcho2 are present; RT-PCR confirms the presence of the appropriate gene-specific amplicons while *in situ* hybridization shows localization in four-cell embryos through shield stage (when gastrulation begins) at ~6 hpf (Fig. S3). After the onset of general zygotic transcription (~3 hpf), both *fcho1* and *fcho2* transcripts are still detectable and increase gradually through the segmentation period to 24 hpf. Both *fcho1* and *fcho2* messages are broadly distributed but, by 24 hpf, regional differences are apparent; expression patterns are therefore overlapping but not identical.

Injecting an initiation codon-targeting *fcho1* antisense morpholino oligonucleotide (MO) (Fig. S4) at the 1-cell stage causes a strong dorsalized phenotype at 24 hpf, where structures originating from the dorsal side predominate with accompanying loss of ventral tissues (Fig. 4a-g). Again, severely affected embryos mirror *snailhouse* and *swirl* mutants. The phenotype is dose dependent with increased lethality at higher MO concentrations. MO efficacy is verified by silencing of an appropriate *fcho1*-GFP reporter (Fig. S4) and the phenotype is not markedly different in *p53* MO-coinjected embryos[37]. Earlier in development, at the end of gastrulation (~10 hpf), the *fcho1* morphants are oblong (Fig, 4h, i), typical of dorsalization[33,34]. These morphological abnormalities accompany gene expression pattern changes diagnostic for dorsalization: the positioning of the hindbrain marker *krox20* reveals laterally-expanded stripes compared with controls, while, in the same embryos, expression of *gata1*, a marker of the ventrally-specified erythroid lineage, is diminished (Fig. 4j-m). Also in line with expansion of dorsal cell fates, regional mRNA expression of the dorsally positioned Bmp antagonist Chordin (Fig. 4n) is widened ventrally in shield stage *fcho1* morphants (Fig. 4o, p). Reciprocally, the lateral *bmp4* expression field is variably reduced ventrally, consistent with suppression of positive feedback of *bmp* expression by Bmp signaling in the ventral region (Fig. 4q, r)[38]. During segmentation, the *fcho1* morphants have laterally broadened somitic mesoderm (Fig. 4s, t) that could reflect delayed/abnormal convergence–extension movements. Defective convergence likely reflects a second function of the Bmp gradient in the gastrula: proper locomotion of cells to the midline by modulating cell adhesion[39].

Administering full-length FCHO1 mRNA together with the *fcho1* MO increases morphologically normal 24 hpf embryos to 67% from 12% with the MO alone (Fig. 4u-y). There is >5 bp mismatch with the FCHO1 RNA (Fig. S4) excluding the coinjected transcript titrates out the *fcho1* MO. Injection of the ΔμHD-encoding (1-610) transcript does not similarly correct development in *fcho1* morphants arguing that the basis for the DV patterning defect is Fcho1 insufficiency and that the intact protein is necessary for proper function.

Because FCHO1 and FCHO2 are functionally redundant[12] a translation-blocking *fcho2* MO was also analyzed. The *fcho2* morphants differ strikingly from *fcho1* despite globally similar expression profiles during early embryogenesis (Fig. S5). The largely distinct developmental defects of the morphants indicate that Fcho1 and Fcho2 regulate separate events during zebrafish gastrulation and segmentation, but may also reflect temporal and regional differences in the expression of the two paralogues. There is evidence of weak overlapping function during embryogenesis: although *fcho1+2* MOs combined do not provoke a gross phenotype distinct from *fcho1* MO alone, the *krox20* lateral expansion, elliptical morphology, and spectrum of dorsalized embryos is slightly more severe in *fcho1+2+p53*-injected embryos than in *fcho1+p53*- treated ones (Fig. S5l-r).

Fcho1 binds to Alk8

As the general *fcho1* MO phenotype mirrors Bmp antagonism, we investigated interaction between Fcho1 and Alk8, an early DV patterning type I receptor for Bmp2b–Bmp7[14,40,41]. A genetic link between *fcho1* and *alk8* is revealed by co-injection of MOs targeting the two transcripts at levels (0.5 ng) that, alone, do not produce many dorsalized embryos (Fig. 5a-e). When combined, mildly dorsalized (C2) embryos result with defective ventral tail fin development that resembles 5 ng *alk8* morphants, suggesting that Alk8 and Fcho1 operate along the same pathway. This conclusion is directly substantiated biochemically. C-terminally myc-tagged Alk8 in detergent lysates from transfected HeLa cells is bound by GST-FCHO1 μHD dose-dependently, along with the other binding partners (Fig. 5f-h). Also, Alk8-myc interacts with the immobilized cognate GST-Fcho1 μHDs (~55% identical) while neither the Fcho2 (Fig. 5f), FCHO2 nor SGIP1 μHD (Fig. S6) bind similarly, despite equivalent eps15 interactions. The strong, differential interaction of the Fcho1/FCHO1 μHD with Alk8 is clearly consistent with the differing phenotypes in *fcho1* or *fcho2* MO embryos. There is no obvious preference of the Fcho1 μHD for binding to CA*Alk8 Q204D mutant[41] over the wild-type receptor (Fig. 5g), whereas the related Alk1 interacts with the μHD comparatively weakly (Fig. S6). The μHD interaction with Alk8 is similar to Hrb binding and both are displaced by the eps15 (595-660) peptide at low concentrations (Fig. 5h); so Alk8 does not appear to use a tyrosine-based sorting signal to engage the Fcho1 μHD.

Injecting *bmp2b+bmp7* mRNA elicits strong ventralization although coinjection with *fcho1+2* MOs results in genetic suppression, with primarily dorsalized embryos resulting (Fig. 6). Ectopic mRNA encoding a phosphomimetic CA*Smad1 also strongly ventralizes, even in the presence of *fcho1+2* MOs (Fig. 6e-g). These epistasis-type experiments place Fcho1 within a genetically specified sequence for Bmp signaling (Fig. 6n). Overall, our data imply that Fcho1 positively regulates ventral specification during embryogenesis by

bridging Alk8 and the clathrin machinery, consistent with expanded pSmad1/5/8 staining in FCHO1 mRNA-injected embryos.

AP-2 loss-of-function

FCHO1/2 are argued to be master actuators of endocytosis, remodeling the initial membrane patch and recruiting eps15 and intersectin prior to AP-2[12]. If FCHO1/2 are compulsory for clathrin-coated vesicle formation, one testable prediction is that the early dorsalizing effect of *fcho1+2* MOs is wholly reflective of clathrin-mediated endocytosis dysfunction in developing embryos. Like Fcho1/2, in *D. rerio* the AP-2 α subunit is encoded by a single gene (*ap2a1*) and is maternally deposited. The transcript is broadly expressed in blastula-, gastrula- and segmentation-stage embryos (Fig. S7a-c) like *fcho1/2*.

Translation blocking *ap2a1* MO (Fig. S4) produces pleomorphic early patterning and axis formation abnormalities and many embryos do not survive to 24 hpf (Fig. 7a-e, S5). Phenotypes of surviving morphants at 24 hpf are classified from mild to arrested (Fig. S7d-i). In the most severe embryos, the epiboly movement of blastomeres toward the vegetal pole slows and blastopore closure with incomplete epiboly results in dysmorphic bulging of the yolk (Fig. 7b, d). This defect persists beyond bud stage (10 hpf) and yolk rupture typically follows 14-19 hpf (Fig. 7d). Surviving arrested embryos are not developmentally delayed because there is no further morphological progression by 24 hpf (Fig. S6h). *ap2a1+p53* MO-coinjected embryos still arrest, while simultaneous injection of the *ap2a1* MO and mouse *ap2a2* mRNA reverts the wild-type morphology (Fig. 7f). A second *ap2a1* and an AP-2 μ2-subunit-targeting MO both cause an analogous phenotype. Epiboly arrest may be due, in part, to defective yolk cell endocytosis as the blastoderm margin moves toward the vegetal pole[42]. Later, in surviving embryos, ectoderm delaminates and gross morphology is indicative of severe patterning defects (Fig. 7l, S6f-h) consistent with the major effect of μ*2* MO in early *Xenopus* embryos[43].

A survey of standard target genes for early development[35] shows serious expression abnormalities. When gastrulation begins Fgf is normally produced from the dorsal organizer and weakly along the margin, but in *ap2a1* (but not *fcho1*) MO embryos *fgf8* transcripts are expanded toward both the ventral and animal poles (Fig. 7g-i). Improper *fgf8* transcription is evident at 30% epiboly (~4.7 hpf). At this stage, there is also precocious hyperactiviation of the phosphatase Dusp6, an Fgf target gene[44]. Abnormal and mislocalized production of *dusp6* in *ap2a1* morphants persists to shield stage and, strikingly, expands far beyond the zone of *fgf8* ligand expression. Coinjecting AP-2 α-subunit mRNA restores the normal *dusp6* expression pattern (Fig. 7j). Expansion of Fgf signaling range in AP-2 compromised embryos is consistent with endocytosis shaping and maintaining this morphogen gradient in the zebrafish gastrula[45,46]. Clear Fgf signaling and phenotypic differences between *ap2a1* and *fcho1+2+p53* morphants are apparent in live transgenic *Tg(Dusp6:d2EGFP)*^{pt6} reporter embryos[47] at the 6-somite stage (Fig. 7k-m). As the *ap2a1* MO embryos are still round, suppressing AP-2 expression must cause additional cellular/regional defects because Fgf receptor hyperactivation typically induces dorsalization[44,48]. Importantly, the GFP reporter rules out that abnormal activation of Fgf signaling underlies the *fcho1* MO dorsalization.

Other body plan patterning pathways are anomalous in *ap2a1*-silenced embryos when gastrulation starts: distribution of *chordin, bmp4, bozozok, goosecoid, and squint* transcripts is abnormal (Fig. 7n-p). Thus, AP-2 appears to function generally in multiple developmental pathways during early development as seriously defective body patterning information results without a functional adaptor. Because the effect on transducing Fgf and other inductive signals in *ap2a1* morphants is distinct from how *fcho1+2* MO alters the fate map, we conclude AP-2 function is not invariably dependent on upstream Fcho1/2 during embryogenesis.

DISCUSSION

Proper embryonic patterning depends on precise temporal integration of spatially complex signaling events. Endocytosis modulates signaling by constantly adjusting surface protein abundance[49] and here we show that this process is vital for zebrafish development. Our results are consistent with Fcho1 operating with Alk8 and Bmp2b–Bmp7 heterodimers to signal ventral fates. Because FCHO1/2 are incontestably clathrin-coat constituents, the simplest model is that clathrin-mediated endocytosis promotes Bmp signaling. The precise basis for this remains to be elucidated; one possibility is that Fcho1/2 with Alk8 shapes the ventral Bmp gradient, as does type I BMP receptor Thick veins in *Drosophila*[50]. Thick veins, the *Drosophila* Decapentaplegic receptor, binds directly to another intersectin-binding EFC domain protein, Nervous wreck[51]. Yet Nervous wreck has a C-terminal SH3 domain substituted for the μHD, so the basis for the interaction cannot be structurally similar, and, critically, the consequence of the association is negative feedback on Decapentaplegic signaling. It thus appears remote that muniscins govern routing of Alk8 receptors to lysosomes because Fcho1 positively modulates Bmp signaling in zebrafish embryos.

Receptors can require prior internalization and recycling to gain signaling competence[52]. Another possibility then is that by promoting uptake of uncomplexed type I receptors (Alk8), the level of type I–II functional heterodimers is optimized. Alternatively, Fcho1 could be involved in forming Bmp gradients by decreasing available receptor/ligand in dorsally positioned cells, but that would give rise to ventralization, not dorsalization, upon MO injection. More likely, clathrin-mediated endocytosis provides access to an endosomal signaling station for cytosolic propagation and refinement of the Bmp signal. Spatial separation between TGF-β/BMP receptor activation at the plasma membrane and signal propagation from endosomes is apparent[53,54]. In cultured cells, the extent of activin-triggered Smad phosphorylation decreases when internalization is blocked[55]. Optimal phosphorylation of R-Smads by TGF-β receptors requires SARA, an endosome-associated PtdIns3P-binding protein[56-59]. The R-Smad binding FYVE domain protein Endofin plays an analogous role during BMP signaling[60]. Fcho1 could drive the delivery of Alk8 to endosomes for an encounter with Endofin then.

Zebrafish are characterized by very rapid developmental progression; tissue specific cell clones are evident during gastrulation (>6 hpf) and a recognizable body plan and differentiating organs apparent before 12 hpf[61]. Perhaps Fcho1/2 has been previously missed because the time constraints for signal propagation in other systems are dissimilar to *D. rerio* early development. An association between FCHO1 and ACVR1, the mammalian

Alk8 ortholog, has been mapped by high-throughput affinity-capture proteomics[62]. Another hallmark of zebrafish embryogenesis is brisk and expansive cell movements. Maximal signal transmission from an endosomal extension of the cell surface may allow proper 'memory' signaling in cells that have moved away from the initial, fate-determining morphogen gradient[63].

On the basis of MOs recapitulating maternal effect phenotypes[33] it is clear the translational silencing approach ablates maternal gene expression. Why then are *fcho1*, *fcho2* and *ap2a1* morphants not more severely affected? Targeted gene disruption of the AP-2 μ2 subunit is lethal[64] but *ap2a1* MO in zebrafish allows visualization of early embryonic processes prior to dysmorphic arrest due to protein insufficiency. This is because MO-based silencing cannot obstruct maternally deposited protein. Substantial clathrin coat machinery must be provisioned in the oocyte as massive cortical granule exocytosis following fertilization is balanced by compensatory clathrin-dependent endocytosis[65]. Clathrin-coated buds are also seen at the cleavage furrow during the initial rounds of cell division following fertilization[66]. Still, an early and severe developmental defect on *ap2a1* silencing is fully consistent with AP-2 μ2 subunit morphants in *Xenopus*[43]. Strikingly the phenotypic outcome of extinguishing AP-2 or Fcho1/2 transcripts is not identical. If Fcho1/2 are obligatory for the nucleation of endocytic clathrin coats, this is unexpected. One possibility is that the perdurance of the muniscins is greater than the AP-2 heterotetramer in early embryos. However, simultaneous RNAi silencing of both FCHO1 and FCHO2 in neither HeLa nor BS-C-1 cells causes loss of AP-2-positive clathrin-coated structures at the cell surface (Fig. 8). This is fully consistent with the very mild phenotype in *syp1*Δ yeast[15,17,18].

The structure, dynamics[7,12,67] and extensive interactions shared by FCHO1 and FCHO2 suggest muniscins advance clathrin endocytosis. This may explain the weak additive effect of *fcho2* MO on the *fcho1* morphant phenotype, reflecting a degree of functional overlap between the paralogues. If part of a pioneer module[7,12], how do clathrin coats persist without these factors? A topological feature of the clathrin interactome is redundancy[2,6]. Surplus connections make the network tolerant to perturbations; AP-2 can be largely extinguished in cultured cells but rapid uptake of certain cargo continues[27,28]. As the μHD engages other pioneer scaffolds (Fig. 2h) collective establishment of this preponderance of links, even without Fcho1/2, permits positioning of AP-2 at the first encounter zone of a bud site. Cargo selective defects are instead manifest, highlighting that all known μHD-bearing proteins are involved in gathering cargo[15].

METHODS

Molecular cloning and constructs

The human *FCHO1*, *FCHO2*, mouse *Fcho2* and zebrafish *Fcho2* cDNA clones were obtained from Open Biosystems. The sequences encoding full-length *FCHO1*, *FCHO1* (1-609), *FCHO1* (267-609), *FCHO1* (442-609), *FCHO1* μHD (609-889), full-length *Fcho2* and *Fcho2* μHD (527-809) were PCR amplified and cloned into pEGFP-C1 or pGEX-4T-1 for expression of either an N-terminal GFP or GST fusion protein. The full-length human *FCHO1*, *FCHO1* (1-609) and zebrafish *fcho2* were similarly cloned into pCS2+ for mRNA synthesis or transient transfections. Stop codons were introduced at appropriate sites using

QuikChange (Stratagene) site-directed mutagenesis to construct FCHO1 (1-275), FCHO1 (1-609), Fcho2 (1-302) and the various other truncation mutants described in the text. The GST-β2 appendage (rat residues 701-937), GST-α_C appendage (mouse residues 701-938), GST-eps15 (595-896) and GST-ARH constructs have been described previously[15,25,68]. The 25-bp regions at the 5′ end of zebrafish *fcho1*, *fcho2* and *ap2a1* used to design antisense morpholinos were cloned in-frame into pCS2-GFP-N1 to generate respective 5′MO-GFP constructs that were subsequently used to test the effectiveness of translational silencing by *fcho1*, *fcho2* and *ap2a1* MOs *in vivo*. The coding sequence of the zebrafish *fcho1* μHD with flanking 5′ and 3′ regions was first amplified by RT-PCR from 1,000-cell stage zebrafish embryonic cDNA using a set of PCR primers designed from EST clones encoding the 5′ (GenBank accession AL920021) or the 3′ (GenBank AL921007) ends of the μHD. Then, the complete coding sequence of the μHD was PCR amplified from the RT-PCR product and cloned into pGEX-4T-1. The pCS2-*alk8*, pCS2-*bmp2b* and pCS2-*bmp7* plasmids[13] were kindly provided by Dr. Mary Mullins while the pCS2-CA**smad1* construct (^{470}SVS of zebrafish Smad1 mutated to ^{470}DVD) was a gift from Dr. Beth Roman. The *alk8* coding sequence was PCR amplified from pCS2-*alk8* and subcloned into the pCS2-myc$_6$ vector to obtain pCS2-*alk8*-myc$_6$. A Q204D mutation yielded the CA*Alk8. All constructs were sequence-verified and full details of plasmids and primers (Integrated DNA Technologies) are available upon request.

RT-PCR and 5′ RACE

Total RNA (5 μg) extracted from embryos at different developmental stages using TRIZOL method (Invitrogen) was used as template for cDNA preparation. cDNA was generated using an oligo-(dT) primer and Thermoscript reverse transcriptase (Invitrogen) according to the manufacturer's directions. Subsequently, the cDNA was amplified with gene specific primers for *fcho1*, *fcho2*, and *ap2a1* (as listed in the Supplementary Table). β actin primers were used as an internal control for the quality of cDNA synthesis. The amplified DNA was subjected to agarose gel electrophoresis and exon-specific bands identified both by size and by sequencing. 5′ RACE was performed by standard procedures (Invitrogen). Total RNA from 1-cell and 1,000-cell stage embryos was reverse transcribed to cDNA using an antisense gene specific primer (GSP1) near the 5′ end. The template cDNA was tailed at 3′ end using dCTP and terminal deoxynucleotidyl transferase (New England Biolabs). The tailed cDNA was PCR amplified with a set composed of a 5′ RACE anchor adaptor primer and a second antisense gene specific primer (GSP2). The primer sequences used for 5′ RACE are provided in the Supplementary Table. The amplicon was purified, confirmed by sequencing and the sequence deposited in GenBank (Accession number JN412732) at the NCBI.

Antibodies

The affinity-purified rabbit anti-FCHO1 antibody 1 (1:2,500), anti-FCHO2 (1:2,500), anti-Dab2 (1:1,000), anti-epsin 1 (1:10,000) and anti-AP-1/2 β1/β2-subunit GD/1 (1:2,500) antibodies were produced commercially for our laboratory. A second affinity-purified anti-FCHO2 (1:2500) antibody was kindly provided by Dr. Harvey McMahon. Affinity-purified rabbit anti-eps15 polyclonal antibody was a gift from Dr. Ernst Ungewickell, the anti-clathrin HC mAbs TD.1 (1:5,000) and X22 and the anti-AP-2 α-subunit mAb AP.6 were

generously provided by Dr. Frances Brodsky, the anti-CALM mAb (1:1,000) kindly provided by Dr. Jeong-Ah Kim, rabbit R11-29 anti-AP-2 μ2-subunit (1:3,000) antiserum kindly provided by Dr. Juan Bonifacino and the rabbit anti-intersectin 1 (1:2,000) antibody a gift from Dr. Peter McPherson. The affinity-purified rabbit anti-APPL1 (1:50) was kindly provided by Dr. David Kaplan. The goat anti-Hrb C-19 (1:1000; sc-1424), rabbit anti-eps15 C-20 (1:500; sc-534) polyclonal antibodies and rabbit anti-SHIP2 mAb E-2 (1:500; sc-166641) from Santa Cruz Biotechnology, rabbit anti-eps15R (1:5,000; EP-1145Y) antibody and rabbit anti-FCHO1 antibody 2 (1:1,000; ab84740) from Abcam, and the mouse anti-myc mAb 9E10 (1: 1,000; MMS-150P) from Covance were used. The anti-β-tubulin mAb E7 (1:2,500) was purchased from the DSHB, mAbs directed against the AP-2 α subunit clone 8/Adaptin α (1:1,000; 610502), AP180 clone 34 (1:250; A41820), amphiphysin I clone 15 (1:5,000; A59420), EEA1 clone C14/EEA1 (1:250; 610457) and intersectin clone 29 (1:250; 611574) were from BD Transduction Laboratories. The secondary antibodies used were donkey anti-rabbit (1:5,000; NA934V) or anti-mouse (1:5,000; NA931V) horseradish peroxidase conjugates from GE Healthcare or rabbit anti-goat (1:5,000; A4174) peroxidase conjugate from Sigma.

Cell culture and transfections

HeLa SS6 cells were cultured in DMEM supplemented with 10% fetal calf serum and 2 mM L-glutamine at 37°C in an atmosphere of 5% CO_2. BS-C-1 cells stably expressing GFP-tagged clathrin light chain a were generously provided by Tomas Kirchhausen. The BS-C-1 cells were similarly grown in DMEM, 10% fetal calf serum, 2 mM L-glutamine supplemented with 0.4 mg/ml G418. Cells were routinely transfected with plasmids using Lipofectamine 2000 (Invitrogen) or siRNA oligonucleotides (listed in Supplementary Table) using Oligofectamine (Invitrogen) according to the manufacturer's instructions. For all RNAi treatments, cells were transfected twice, normally 48 h apart and with reseeding the cells before the second siRNA application, at which time the relevant transiently transfected plasmid was also included. Typically, 18-24 h after the second transfection, cells were fixed with 4% paraformaldehyde, blocked and permeabilized in 10% normal goat serum, 0.2% saponin in PBS. For transferrin binding and uptake assays, cells were incubated in DMEM, 25 mM Hepes, 0.5% BSA for 1 h at 37°C to remove bound transferrin. Alternatively, lysates from parental HeLa cells or HeLa cells expressing (from pCS2+) full-length (1-889) or truncated (1-609) *H. sapiens* FCHO1, or myc-tagged WT Alk8 or CA*Alk8 were prepared from transiently-transfected (24-48 h) cells collected by trypsinization. After washing, cell pellets were solubilized on ice for 30 min in 25 mM Hepes-KOH (pH 7.2), 125 mM potassium acetate, 5 mM magnesium acetate, 2 mM EDTA, 2mM EGTA, and 2 mM dithiothreitol (assay buffer) supplemented with 1% Triton X-100, 1 mM PMSF and Complete protease inhibitor cocktail (Roche). Lysates were centrifuged at 20,000 X g_{max} before use in binding assays.

Zebrafish maintenance, morpholinos and mRNA injections

The Oregon AB* and *Tg(Dusp6:d2EGFP)*^{pt6} strains were maintained under standard conditions at the University of Pittsburgh School of Medicine in accordance with Institutional and Federal guidelines for use, care and maintenance of experimental animal models and with University of Pittsburgh Institutional Animal Care and Use Committee

(IACUC) approval. Embryos from natural matings were obtained and developmentally staged[61]. The sequence of the various morpholinos used in this study, custom synthesized by Gene Tools, are listed in the Supplementary Table. The translation-blocking ATG specific *fcho1* morpholino was designed on the basis of the authentic 5′ sequence of zebrafish embryonic *fcho1* transcript mapped by 5′ RACE. A standard control MO and *p53* MO was obtained from Gene Tools as detailed elsewhere[69]. The desired concentrations of the appropriate morpholinos were microinjected at 5 nl/embryo into the yolk at 1- to 2-cell stage. Capped mRNAs for misexpression and rescue experiments were transcribed *in vitro* from linearized pCS2+ constructs using SP6 mMessage mMachine kit (Ambion) and microinjected at 1 nl into the blastomere at 1-cell stage. After injections, the embryos were incubated in E3 medium (5 mM NaCl, 0.17 mM KCl, 0.33 mM $CaCl_2$, 0.33 mM $MgSO_4$, 0.01% methylene blue) at 28°C until the desired stage.

Whole-mount *in situ* hybridization and immunofluorescence

The EST clones for *fcho1* (GenBank AL920021) and *ap2a1* (GenBank AL920300) in pBluescript SK+ were obtained from Open Biosystems, linearized and directly used for riboprobe synthesis. For *fcho2*, an 880-bp fragment encoding the C-terminal end was PCR amplified (using *fcho2* T7 sense and antisense primers) from the zebrafish *fcho2* EST clone (GenBank BC095680). All other probes used in this study (no tail, sonic hedgehog, bmp4, chordin, krox20, gata1, goosecoid, bozozok, squint, fgf8, fgfR1 and *dusp6*) were made similarly by linearizing corresponding vectors containing a T7 RNA polymerase promoter, using appropriate restriction enzymes as described elsewhere[47,69]. Riboprobe synthesis for *in situ* hybridization was performed using DIG RNA labeling mix and T7 RNA polymerase (Roche) according to the manufacturer's recommendations. Zebrafish embryos at appropriate developmental stages were fixed in 4% paraformaldehyde at 4°C overnight, washed once in PBS and stored in methanol at -20°C. Whole-mount *in situ* hybridizations were performed by standard procedures[69]. Embryos were washed several times in PBS and mounted in glycerol. Alternatively, live embryos, either within or removed from the chorion, were mounted in 3% methylcellulose and overlaid with E3 containing 0.016% tricaine (pH 7.0). Oriented embryos were viewed using a Leica MZ16FA stereo fluorescence microscope with a 1x (NA 0.14) objective and bright field or fluorescence images collected with a QImaging Retiga-EXi Fast 1394 digital camera.

For immunofluorescence, embryos fixed overnight in 4% paraformaldehyde at 4°C, were permeabilized in 1% Triton-X-100, blocked in 10% sheep serum, 1% DMSO, 0.1% Triton X-100 in PBS and probed overnight with rabbit anti-phosphoSmad (pSmad) 1/5/8 (1:100; 9511) from Cell Signaling Technology or GD/1 (1:100) antibody. The immunizing peptide for the GD/1 antibody (GDLLNLLGPPV) is 100% conserved in the *D. rerio* AP-2 β2 subunit (*ap2b1*). Primary antibodies were followed with goat anti-rabbit Alexa488-or Cy5-conjugated antibody (1:500; Molecular Probes) and Hoechst 33258 nuclear stain before mounting for confocal microscopy. For GFP-FCHO1/AP-2 immunofluorescence, embryos at 5 hpf were embedded in 1% low melting point agarose in E3 medium on poly-D-lysine coated dishes (MatTek) with the animal pole oriented toward the glass bottom. For pSmad 1/5/8 immunofluorescence, embryos at 7 hpf were embedded with dorsal shield side toward the right. Images were acquired on an Olympus Fluoview1000 confocal microscope using an

UplanSapo 20X (NA 0.75) or an UPlanFLN 40X (NA 1.3) oil objective. Data was acquired using the FV10-ASW software. Similar procedures were used for immunofluorescence analysis of cultured mammalian cells.

Supplementary Material

Refer to Web version on PubMed Central for supplementary material.

Acknowledgements

We are indebted to our many gracious colleagues for generously providing important reagents that were essential for this study. Supported by NIH grants R01 HL088016 (MT) and R01 GM60979 (BW) and R01 DK53249 (LMT).

REFERENCES

1. Conner SD, Schmid SL. Regulated portals of entry into the cell. Nature. 2003; 422:37–44. [PubMed: 12621426]
2. McMahon HT, Boucrot E. Molecular mechanism and physiological functions of clathrin-mediated endocytosis. Nat Rev Mol Cell Biol. 2011; 12:517–533. doi:nrm3151 [pii] 10.1038/nrm3151. [PubMed: 21779028]
3. Kirchhausen T. Imaging endocytic clathrin structures in living cells. Trends Cell Biol. 2009; 19:596–605. doi:S0962-8924(09)00192-5 [pii] 10.1016/j.tcb.2009.09.002. [PubMed: 19836955]
4. Kelly BT, Owen DJ. Endocytic sorting of transmembrane protein cargo. Curr Opin Cell Biol. 2011 doi:S0955-0674(11)00021-4 [pii] 10.1016/j.ceb.2011.03.004.
5. Reider A, Wendland B. Endocytic adaptors - social networking at the plasma membrane. J Cell Sci. 2011; 124:1613–1622. doi:124/10/1613 [pii] 10.1242/jcs.073395. [PubMed: 21536832]
6. Traub LM. Tickets to ride: selecting cargo for clathrin-regulated internalization. Nat. Rev. Mol. Cell Biol. 2009; 10:583–596. [PubMed: 19696796]
7. Taylor MJ, Perrais D, Merrifield CJ. A high precision survery of the molecular dynamics of mammalian clathrin mediated endocytosis. PLoS Biol. 2011; 9:e1000604. [PubMed: 21445324]
8. Schmid EM, McMahon HT. Integrating molecular and network biology to decode endocytosis. Nature. 2007; 448:883–888. [PubMed: 17713526]
9. Boucrot E, Saffarian S, Massol R, Kirchhausen T, Ehrlich M. Role of lipids and actin in the formation of clathrin-coated pits. Exp. Cell Res. 2006; 312:4036–4048. [PubMed: 17097636]
10. Zoncu R, et al. Loss of endocytic clathrin-coated pits upon acute depletion of phosphatidylinositol 4,5-bisphosphate. Proc. Natl. Acad. Sci. U S A. 2007; 104:3793–3798. [PubMed: 17360432]
11. Jackson LP, et al. A large-scale conformational change couples membrane recruitment to cargo binding in the AP2 clathrin adaptor complex. Cell. 2010; 141:1220–1229. doi:S0092-8674(10)00542-8 [pii] 10.1016/j.cell.2010.05.006. [PubMed: 20603002]
12. Henne WM, et al. FCHo proteins are nucleators of clathrin-mediated endocytosis. Science. 2010; 328 doi:science.1188462 [pii] 10.1126/science.1188462.
13. Little SC, Mullins MC. Bone morphogenetic protein heterodimers assemble heteromeric type I receptor complexes to pattern the dorsoventral axis. Nat. Cell Biol. 2009; 11:637–643. [PubMed: 19377468]
14. Mintzer KA, et al. Lost-a-fin encodes a type I BMP receptor, Alk8, acting maternally and zygotically in dorsoventral pattern formation. Development. 2001; 128:859–869. [PubMed: 11222141]
15. Reider A, et al. Syp1 is a conserved endocytic adaptor that contains domains involved in cargo selection and membrane tubulation. EMBO J. 2009; 28:3103–3016. [PubMed: 19713939]
16. Katoh M. Identification and characterization of human FCHO2 and mouse Fcho2 genes in silico. Int. J. Mo.l Med. 2004; 14:327–331.
17. Stimpson HE, Toret CP, Cheng AT, Pauly BS, Drubin DG. Early-arriving Syp1p and Ede1p function in endocytic site placement and formation in budding yeast. Mol. Biol. Cell. 2009

18. Boettner DR, et al. The F-BAR protein Syp1 negatively regulates WASp-Arp2/3 complex activity during endocytic patch formation. Curr. Biol. 2009; 19:1979–1987. [PubMed: 19962315]
19. Uezu A, et al. Characterization of the EFC/F-BAR domain protein, FCHO2. Genes Cells. 2011 doi:10.1111/j.1365-2443.2011.01536.x.
20. Zoncu R, et al. A phosphoinositide switch controls the maturation and signaling properties of APPL endosomes. Cell. 2009; 136:1110–1121. [PubMed: 19303853]
21. Henne WM, et al. Structure and analysis of FCHo2 F-BAR domain: a dimerizing and membrane recruitment module that effects membrane curvature. Structure. 2007; 15:839–852. [PubMed: 17540576]
22. Edeling MA, Smith C, Owen D. Life of a clathrin coat: insights from clathrin and AP structures. Nat. Rev. Mol. Cell Biol. 2006; 7:32–44. [PubMed: 16493411]
23. Edeling MA, et al. Molecular switches involving the AP-2 β2 appendage regulate endocytic cargo selection and clathrin coat assembly. Dev. Cell. 2006; 10:329–342. [PubMed: 16516836]
24. Schmid EM, et al. Role of the AP2 β-appendage hub in recruiting partners for clathrin coated vesicle assembly. PLoS Biol. 2006; 4:e262. [PubMed: 16903783]
25. Mishra SK, et al. Dual-engagement regulation of protein interactions with the AP-2 adaptor α appendage. J. Biol. Chem. 2004; 279:46191–46203. [PubMed: 15292237]
26. Praefcke GJ, et al. Evolving nature of the AP2 α-appendage hub during clathrin-coated vesicle endocytosis. EMBO J. 2004; 23:4371–4383. [PubMed: 15496985]
27. Hinrichsen L, Harborth J, Andrees L, Weber K, Ungewickell EJ. Effect of clathrin heavy chain- and α-adaptin specific small interfering RNAs on endocytic accessory proteins and receptor trafficking in HeLa cells. J. Biol. Chem. 2003; 278:45160–45170. [PubMed: 12960147]
28. Motley A, Bright NA, Seaman MN, Robinson MS. Clathrin-mediated endocytosis in AP-2-depleted cells. J. Cell Biol. 2003; 162:909–918. [PubMed: 12952941]
29. Uezu A, et al. SGIP1α is an endocytic protein that directly interacts with phospholipids and Eps15. J. Biol. Chem. 2007; 282:26481–26489. [PubMed: 17626015]
30. Yamabhai M, et al. Intersectin, a novel adaptor protein with two Eps15 homology and five Src homology 3 domains. J. Biol. Chem. 1998; 273:31401–31407. [PubMed: 9813051]
31. Koh TW, et al. Eps15 and Dap160 control synaptic vesicle membrane retrieval and synapse development. J. Cell Biol. 2007; 178:309–322. [PubMed: 17620409]
32. Sengar AS, Wang W, Bishay J, Cohen S, Egan SE. The EH and SH3 domain Ese proteins regulate endocytosis by linking to dynamin and Eps15. EMBO J. 1999; 18:1159–1171. [PubMed: 10064583]
33. Imai Y, Talbot WS. Morpholino phenocopies of the bmp2b/swirl and bmp7/snailhouse mutations. Genesis. 2001; 30:160–163. [PubMed: 11477698]
34. Mullins MC, et al. Genes establishing dorsoventral pattern formation in the zebrafish embryo: the ventral specifying genes. Development. 1996; 123:81–93. [PubMed: 9007231]
35. Schier AF, Talbot WS. Molecular genetics of axis formation in zebrafish. Annu. Rev. Genet. 2005; 39:561–613. [PubMed: 16285872]
36. Tucker JA, Mintzer KA, Mullins MC. The BMP signaling gradient patterns dorsoventral tissues in a temporally progressive manner along the anteroposterior axis. Dev Cell. 2008; 14:108–119. doi:S1534-5807(07)00424-8 [pii] 10.1016/j.devcel.2007.11.004. [PubMed: 18194657]
37. Robu ME, et al. p53 activation by knockdown technologies. PLoS Genet. 2007; 3:e78. [PubMed: 17530925]
38. Schulte-Merker S, Lee KJ, McMahon AP, Hammerschmidt M. The zebrafish organizer requires chordino. Nature. 1997; 387:862–863. doi:10.1038/43092. [PubMed: 9202118]
39. von der Hardt S, et al. The Bmp gradient of the zebrafish gastrula guides migrating lateral cells by regulating cell-cell adhesion. Curr. Biol. 2007; 17:475–487. [PubMed: 17331724]
40. Bauer H, Lele Z, Rauch GJ, Geisler R, Hammerschmidt M. The type I serine/threonine kinase receptor Alk8/Lost-a-fin is required for Bmp2b/7 signal transduction during dorsoventral patterning of the zebrafish embryo. Development. 2001; 128:849–858. [PubMed: 11222140]
41. Payne TL, Postlethwait JH, Yelick PC. Functional characterization and genetic mapping of alk8. Mech. Dev. 2001; 100:275–289. [PubMed: 11165484]

42. Solnica-Krezel L. Gastrulation in zebrafish — all just about adhesion? Curr. Opin. Genet. Dev. 2006; 16:433–441. [PubMed: 16797963]
43. Borner GH, et al. CVAK104 is a novel regulator of clathrin-mediated SNARE sorting. Traffic. 2007; 8:893–903. doi:TRA576 [pii] 10.1111/j.1600-0854.2007.00576.x. [PubMed: 17587408]
44. Tsang M, et al. A role for MKP3 in axial patterning of the zebrafish embryo. Development. 2004; 131:2769–2779. [PubMed: 15142973]
45. Yu SR, et al. Fgf8 morphogen gradient forms by a source-sink mechanism with freely diffusing molecules. Nature. 2009; 461:533–536. [PubMed: 19741606]
46. Scholpp S, Brand M. Endocytosis controls spreading and effective signaling range of Fgf8 protein. Curr. Bio.l. 2004; 14:1834–1841. doi:S0960982204007481 [pii] 10.1016/j.cub.2004.09.084.
47. Molina GA, Watkins SC, Tsang M. Generation of FGF reporter transgenic zebrafish and their utility in chemical screens. BMC Dev. Biol. 2007; 7:62. [PubMed: 17553162]
48. Furthauer M, Van Celst J, Thisse C, Thisse B. Fgf signalling controls the dorsoventral patterning of the zebrafish embryo. Development. 2004; 131:2853–2864. doi:10.1242/dev.01156 dev.01156 [pii]. [PubMed: 15151985]
49. Sorkin A, von Zastrow M. Endocytosis and signalling: intertwining molecular networks. Nat. Rev. Mol. Cell Biol. 2009; 10:609–922. [PubMed: 19696798]
50. Belenkaya TY, et al. Drosophila Dpp morphogen movement is independent of dynamin-mediated endocytosis but regulated by the glypican members of heparan sulfate proteoglycans. Cell. 2004; 119:231–244. doi:S0092867404009390 [pii] 10.1016/j.cell.2004.09.031. [PubMed: 15479640]
51. O'Connor-Giles KM, Ho LL, Ganetzky B. Nervous wreck interacts with thickveins and the endocytic machinery to attenuate retrograde BMP signaling during synaptic growth. Neuron. 2008; 58:507–518. [PubMed: 18498733]
52. Wang W, Struhl G. Distinct roles for Mind bomb, Neuralized and Epsin in mediating DSL endocytosis and signaling in Drosophila. Development. 2005; 132:2883–2894. [PubMed: 15930117]
53. Hartung A, et al. Different routes of bone morphogenic protein (BMP) receptor endocytosis influence BMP signaling. Mol Cell Biol. 2006; 26:7791–7805. doi:MCB.00022-06 [pii] 10.1128/MCB.00022-06. [PubMed: 16923969]
54. Heining E, Bhushan R, Paarmann P, Henis YI, Knaus P. Spatial segregation of BMP/Smad signaling affects osteoblast differentiation in C2C12 cells. PLoS One. 2011; 6:e25163. doi:10.1371/journal.pone.0025163 PONE-D-11-09166 [pii]. [PubMed: 21998639]
55. Zhou Y, et al. Receptor internalization-independent activation of Smad2 in activin signaling. Mol. Endocrinol. 2004; 18:1818–1826. [PubMed: 15087470]
56. Tsukazaki T, Chiang TA, Davison AF, Attisano L, Wrana JL. SARA, a FYVE domain protein that recruits Smad2 to the TGFb receptor. Cell. 1998; 95:779–791. doi:S0092-8674(00)81701-8 [pii]. [PubMed: 9865696]
57. Lin HK, Bergmann S, Pandolfi PP. Cytoplasmic PML function in TGF-beta signalling. Nature. 2004; 431:205–211. doi:10.1038/nature02783 nature02783 [pii]. [PubMed: 15356634]
58. Di Guglielmo GM, Le Roy C, Goodfellow AF, Wrana JL. Distinct endocytic pathways regulate TGF-beta receptor signalling and turnover. Nat. Cell Biol. 2003; 5:410–421. [PubMed: 12717440]
59. Hayes S, Chawla A, Corvera S. TGF beta receptor internalization into EEA1-enriched early endosomes: role in signaling to Smad2. J. Cell Biol. 2002; 158:1239–1249. [PubMed: 12356868]
60. Shi W, et al. Endofin acts as a Smad anchor for receptor activation in BMP signaling. J Cell Sci. 2007; 120:1216–1224. doi:jcs.03400 [pii] 10.1242/jcs.03400. [PubMed: 17356069]
61. Kimmel CB, Ballard WW, Kimmel SR, Ullmann B, Schilling TF. Stages of embryonic development of the zebrafish. Dev. Dyn. 1995; 203:253–310. [PubMed: 8589427]
62. Barrios-Rodiles M, et al. High-throughput mapping of a dynamic signaling network in mammalian cells. Science. 2005; 307:1621–1625. [PubMed: 15761153]
63. Jullien J, Gurdon J. Morphogen gradient interpretation by a regulated trafficking step during ligand-receptor transduction. Genes Dev. 2005; 19:2682–2694. doi:gad.341605 [pii] 10.1101/gad.341605. [PubMed: 16260495]

64. Mitsunari T, et al. Clathrin adaptor AP-2 is essential for early embryonal development. Mol. Cell. Biol. 2005; 25:9318–9323. [PubMed: 16227583]

65. Hart NH, Collins GC. An electron-microscope and freeze-fracture study of the egg cortex of Brachydanio rerio. Cell Tissue Res. 1991; 265:317–328. [PubMed: 1934030]

66. Feng B, Schwarz H, Jesuthasan S. Furrow-specific endocytosis during cytokinesis of zebrafish blastomeres. Exp. Cell Res. 2002; 279:14–20. doi:S0014482702955795 [pii]. [PubMed: 12213209]

67. von Kleist L, et al. Role of the clathrin terminal domain in regulating coated pit dynamics revelaed by small molecule inhibition. Cell. 2011; 146:471–484. doi:S0092-8674(11)00667-2 [pii] 10.1016/j.cell.2011.06.025. [PubMed: 21816279]

68. Thieman JR, et al. Clathrin regulates the association of PIPKIγ661 with the AP-2 adaptor β2 appendage. J. Biol. Chem. 2009; 284:13924–13939. [PubMed: 19287005]

69. Edeling MA, et al. Structural requirements for PACSIN/Syndapin operation during zebrafish embryonic notochord development. PLoS One. 2009; 4:e8150. [PubMed: 19997509]

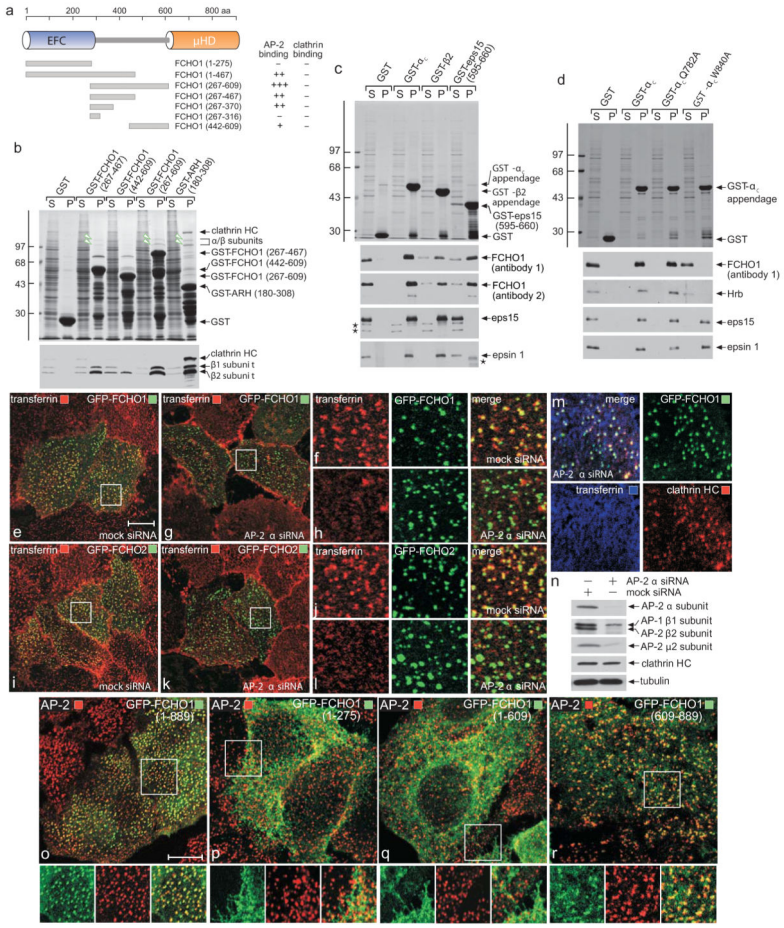

Figure 1.

Binding properties of FCHO1

(**a**) Cartoon of FCHO1 with the location and relative binding properties of the various truncations tested.

(**b**) Coomassie-stained gel and blot of supernatant (S) and pellet (P) fractions of a GST pull-down assay with brain cytosol and immobilized GST or the indicated GST-FCHO1 or GST-ARH fragments. Immunoblotted with anti-clathrin heavy chain (HC) and AP-1/2 β1/2-subunit antibodies. Molecular mass standards (kDa) are shown, and large adaptor subunits (arrowheads) indicated.

(**c**) Pull-down assay with FCHO1 overexpressing HeLa cell lysate and immobilized GST or the indicated GST-fusion proteins. Two independent anti-FCHO1 antibodies used for detection. Non-specific bands (asterisks) are indicated.

(**d**) Pull-down assay with FCHO1 overexpressing HeLa lysates and immobilized GST, GST-α_C appendage or the indicated α_C appendage point mutants.

(**e-l**) Mock or AP-2 α-subunit siRNA-treated HeLa cells transfected with either GFP-FCHO1 or GFP-FCHO2 as indicated were incubated with Alexa568 transferrin on ice before fixation. Representative confocal images show AP-2 silencing leads to loss of transferrin clusters on the surface. Insets (f,h,i,l) provide color-separated and merged enlargements of boxed regions. Scale bar: 10 μm.

(**m**) Confocal image of a region of an AP-2 α-subunit siRNA transfected HeLa cell also expressing GFP-FCHO1. Prior to fixation and staining with an anti-clathrin HC mAb, the silenced cells were incubated at 37°C with 25 μg/ml Alexa633-labeled transferrin.
(**n**) Biochemical assessment of AP-2 siRNA silencing in HeLa cell lysates by immunoblotting.
(**o**-**r**) Representative confocal images of the intracellular localization of full-length (1-889), EFC domain (1-275), ΔμHD (1-609) or μHD (609-889) GFP-tagged FCHO1 compared with AP-2 (α subunit). Insets provide color-separated and merged enlargements of boxed regions. Scale bar: 10 μm.

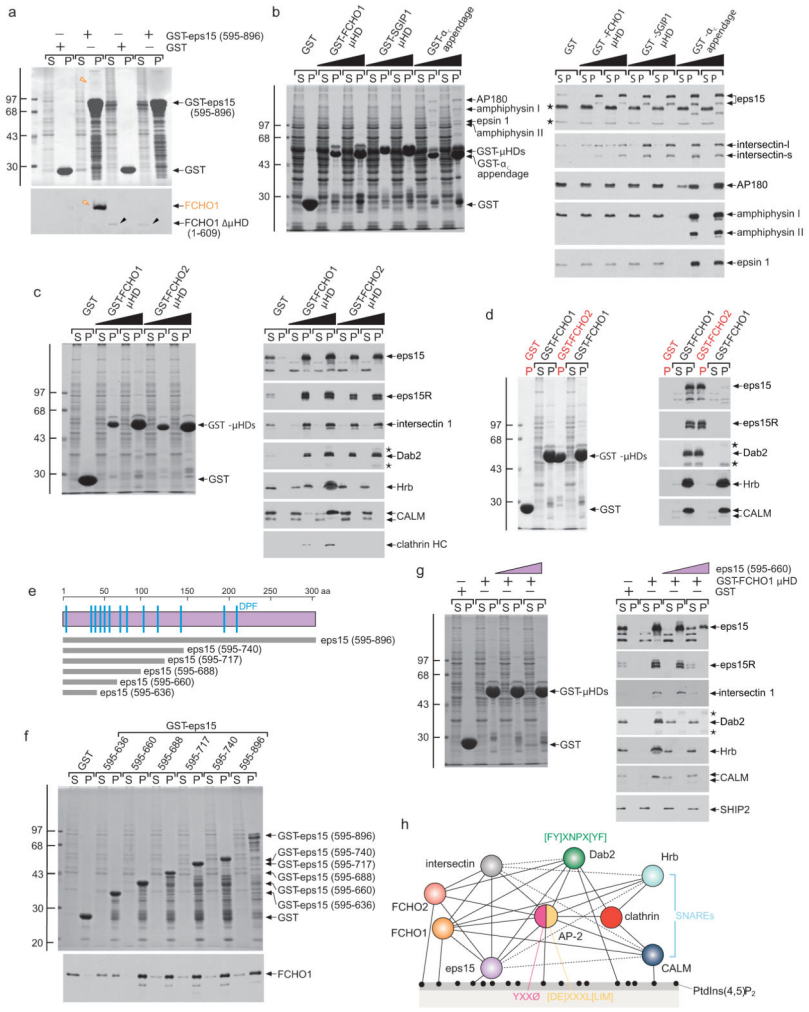

Figure 2.

The μHD interaction hub

(**a**) Coomassie-stained gel and blot of supernatant (S) and pellet (P) fractions of a pull-down assay with full-length or ΔμHD (1-609) FCHO1 overexpressing HeLa lysates and immobilized GST or GST-eps15 (595-896). Immunoblot with anti-FCHO1. Molecular mass standards (kDa) and intact FCHO1 (orange) and ΔμHD (black arrowheads) FCHO1 are indicated.

(**b**) Pull-down assay using brain cytosol and either GST or 50 or 100 μg of the GST-μHD fusions indicated or the GST- α_C appendage. Replicate immunoblots probed with the indicated antibodies with non-specific bands (asterisks) indicated.

(**c**) Pull-down assay using HeLa lysate and either GST or 50 or 100 μg of the GST-μHD fusions indicated. Non-specific bands (asterisks) are indicated. All the GST-μHDs bind to eps15, eps15R, intersectin and Dab2 but only the FCHO1 μHD associates with Hrb, CALM, and clathrin. Note that different eps15 splice isoforms are present in HeLa lysates compared with brain (b).

(**d**) Stained gel and replicate blots of first-stage assay pellets (red P) from incubations of brain cytosol with either GST or GST-FCHO2 μHD compared with supernatant (S) and

pellets (P) from subsequent second-stage pull-downs with the supernatant fractions resulting from the first-stage incubations.

(**e**) Cartoon of the eps15 C terminus with the relative positioning of the various truncations used indicated.

(**f**) Pull-down assay using FCHO1 overexpressing HeLa lysate and the indicated GST-eps15 C-terminal fusions. Immunoblot with anti-FCHO1.

(**g**) Stained gel and replicate blots from pull-down assays with GST or GST-FCHO1 μHD and HeLa lysates supplemented with 5 or 25 μM eps15 (595-660) peptide as indicated.

(**h**) Interaction diagram for FCHO1/2 and select endocytic pioneer coat components. Presumptive contacts are indicated with dotted lines.

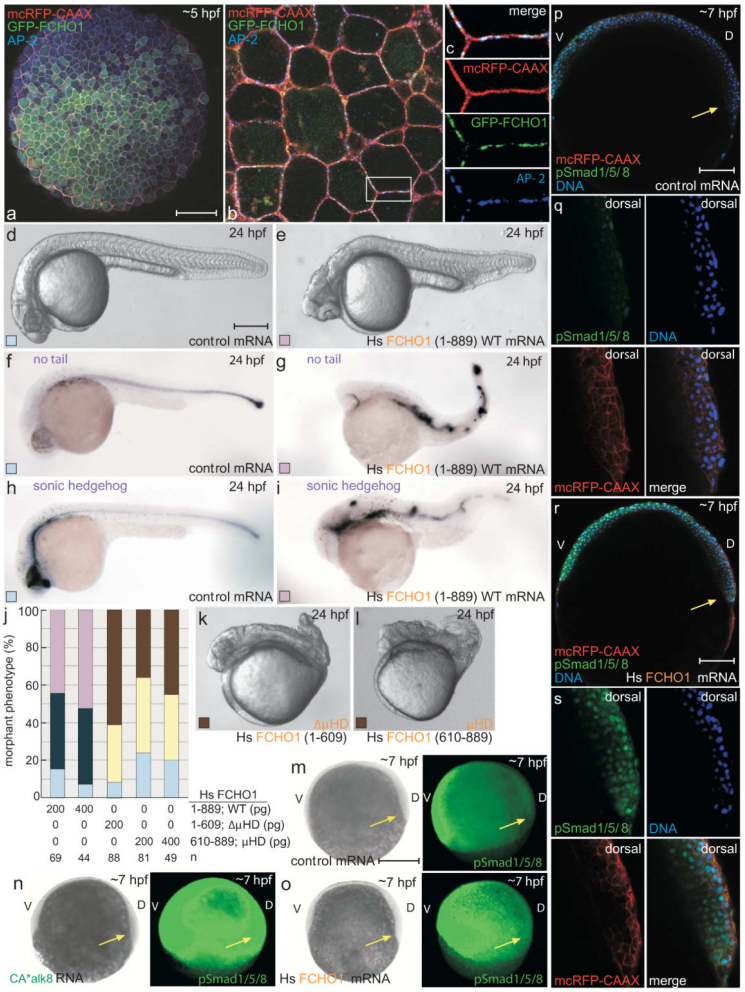

Figure 3.

Developmental defects upon *FCHO1* overexpression

(**a-c**) Representative confocal optical section of 30% epiboly-stage (~5 hpf) embryo injected with a mcRFP-CAAX surface marker (80 pg) and GFP-FCHO1 (400 pg) mRNA after fixation and staining with an anti-AP-2 β2 subunit antibody. Subcellular localization (b) and color-separated enlargements (c) of the boxed region. Scale bar: 125 μm.

(**d-i**) Representative morphology of 80 pg control or 200 pg human (*Hs*) *FCHO1* mRNA-injected embryos at 24 hpf with *no tail* and *sonic hedgehog* mRNA expression patterns. Scale bar: 250 μm.

(**j**) Quantitation of normal (pale blue), mild (navy blue) and moderate (violet) ventralized, or mild (yellow) and severe (brown) mRNA overexpression-induced dorsalized phenotypes, color-coded as in d-i. See Fig. 4 and 6 for complete categorization of the dorsalized and ventralized phenotypic classes.

(**k-l**) Representative morphology of severely affected 200 pg truncated *FCHO1* mRNA-expressing embryos.

(**m-s**) pSmad1/5/8 localization in control (m, p, q), CA**alk8* (5 pg; n) or *FCHO1* (400 pg; o, r, s) mRNA-injected early gastrulation embryos co-injected with 50 pg mcRFP-CAAX.

Wide field (m-o; left) and fluorescence images (m-o; right)) or representative confocal sections (p, r) with color separated and merged enlargements (q, s) of the dorsal organizer region (arrows) shown. D, dorsal; V, ventral. Scale bars: 250 μm (m-o) or 125 μm (p, r).

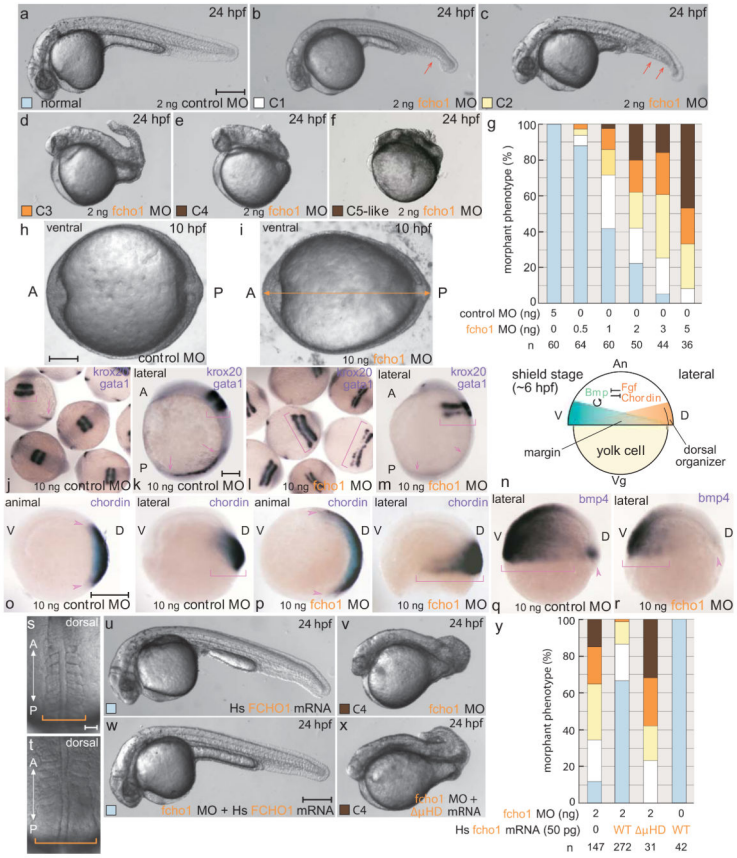

Figure 4.

Fcho1 participates in early embryonic development

(**a-f**) Representative images of the morphant phenotypic range on injection with 2 ng control or 2 ng *fcho1* MO. C5-like morphants are rare and are grouped with the C4 class. Arrows: ventral fin defects. Scale bar: 250 μm.

(**g**) Quantitation of dose-dependent *fcho1* morphant phenotypes at 24 hpf, color coded as in a-f.

(**h-i**) Typical vegetal pole view of 10 ng control or 10 ng *fcho1* early-stage morphants at 10 hpf. A, anterior; P, posterior. Arrow: expanded A-P axis. Scale bar: 125 μm.

(**j-m**) Representative mRNA expression patterns of both *krox20* (brackets) and *gata1* (arrows) in control (j, k) or 10 ng *fcho1* MO-injected (l, m) 5-somite stage embryos. A, anterior; P, posterior. Group dorsal survey view: j, l; individual lateral view: k, m. Scale bar: 225 μm (j and l) or 125 μm (k, m).

(**n**) Schematic cartoon depiction of the general location of opposing morphogen gradients that dictate DV patterning at shield stage. An, animal pole; Vg, vegetal pole; D, dorsal; V, ventral.

(**o-r**) Representative mRNA expression patterns of indicated genes in 10 ng control (o and q) or *fcho1* (p and r) shield-stage morphants. Relative expression zones (arrowhead in animal and bracket in lateral views) shown. Scale bar: 250 μm.

(**s-t**) Dorsal view of gross morphology of developing notochord and somite regions of live 10 ng control (R) and *fcho1* (S) morphants at the 6-somite stage. Scale bar: 50 μm.

(**u**-**x**) representative phenotypes of 2 ng *fcho1* morphants coinjected with indicated human (*Hs*) *FCHO1* mRNA. Scale bar: 250 μm.

(**y**) Quantitation of morphant phenotypes at 24 hpf.

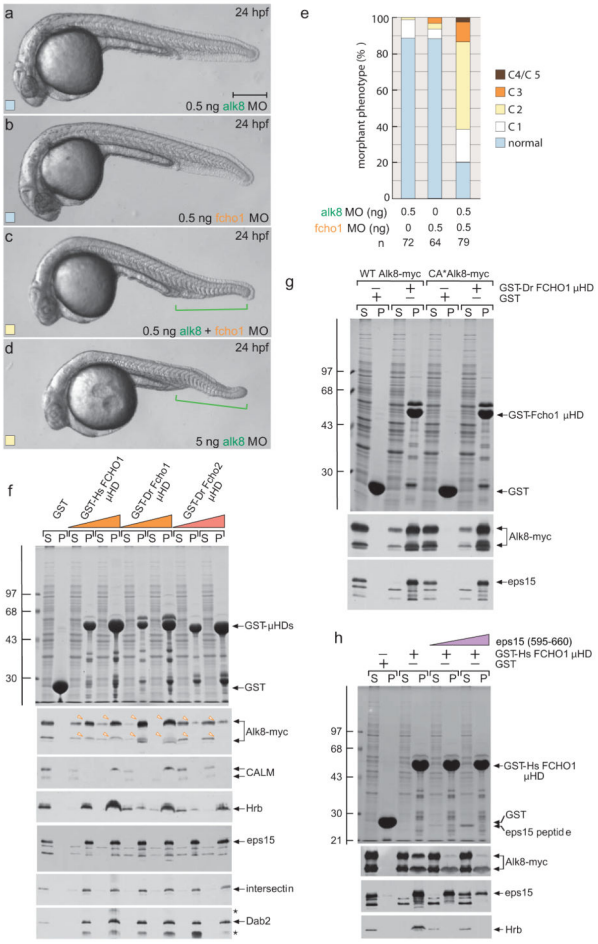

Figure 5.

The Fcho1–Alk8 association

(**a**-**d**). Representative images of live 24 hpf embryos after injection of 0.5 or 5 ng *alk8* MO, 0.5 ng *fcho1* MO or 0.5 ng each of *alk8*+*fcho1* MOs. Defective ventral tail fin is bracketed (green). Scale bar: 250 µm.

(**e**) Quantitation of single and double morphant phenotypes at 24 hpf.

(**f**) Coomassie-stained gel and replicate blots from a pull-down assay using Alk8-myc overexpressing HeLa cell lysate and 150 µg immobilized GST or 50 or 150 µg human (*Hs*) GST-FCHO1 µHD or *D. rerio* (*Dr*) GST-Fcho1 or GST-Fcho2 µHDs. Alk8 (arrowheads in pellet (P) fractions) immunoblot with anti-myc. Note both bands of expressed Alk8-myc, probably differentially *N*-glycosylated forms, bind to the FCHO1/Fcho1 µHD. Non-specific bands (asterisks) are indicated.

(**g**) Pull-down assay using wild-type (WT) or CA*Alk8-myc overexpressing HeLa cell lysate and immobilized GST or GST-*Dr* Fcho1 µHD.

(**h**) Pull-down assay using Alk8-myc overexpressing HeLa cell lysate and immobilized GST or GST-*Hs* FCHO1 µHD. Addition of the eps15 (595-660) competitor peptide (5 or 25 µM) is indicated.

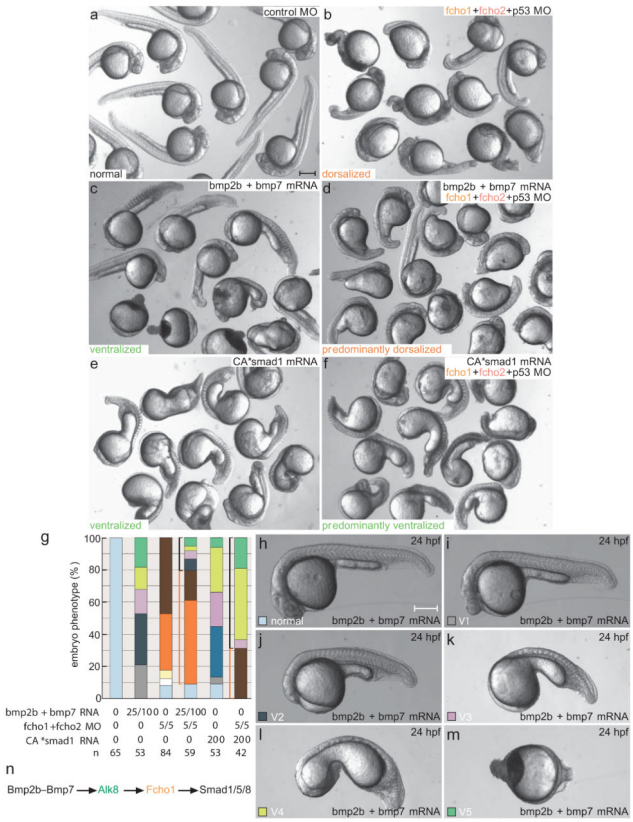

Figure 6.

Fcho1 operates in a genetic Bmp-to-Smad signaling pathway

(**a-f**) Group survey views of comparative morphology of injected control, 25 pg *bmp2b* with 100 pg *bmp7* mRNA, 5 ng each of *fcho1+2+p53* MOs, *bmp2b+bmp7* mRNA along with the *fcho1+2+p53* MOs, 200 pg CA**smad1* mRNA, or the CA**smad1* mRNA along with the *fcho1+2+p53* MOs-injected embryos at 24 hpf. Scale bar: 250 μm.

(**g**) Quantitation of mRNA injected gain-of function (ventralized; black bracketed) and morphant (dorsalized; orange bracketed) phenotypes. The relevant unit for injected mRNA is pg and for MO is ng.

(**h-m**) Representative images of the range and classification of ventralization phenotypes induced by injection of 25 pg *bmp2b* with 100 pg *bmp7* mRNA at the 1-cell stage. Scale bar: 250 μm.

(**n**) Schematic of the linear Bmp-dependent signaling pathway including the relative positioning of Fcho1.

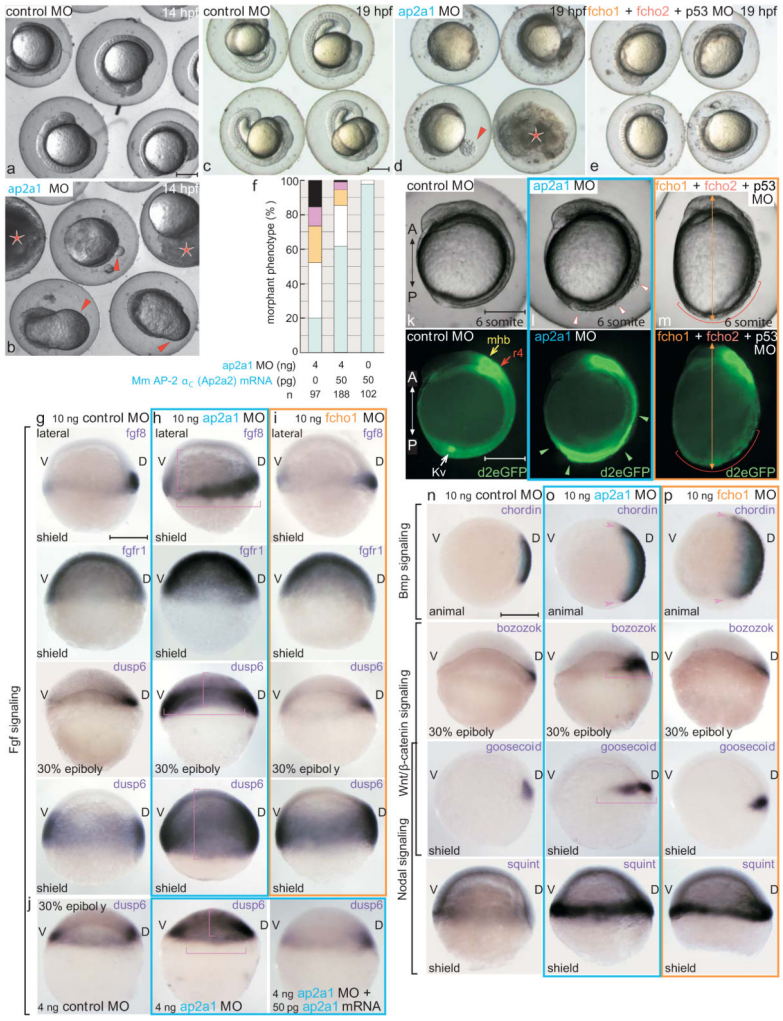

Figure 7.

AP-2 morphants are unlike *fcho1+2* double morphants

(**a**-**e**) Representative survey views of comparative morphology of 10 ng control, *ap2a1* or *fcho1+2+p53* morphants at 14 (a, b) and 19 (c-e) hpf. Extruded yolk (arrowheads) and exploded/disintegrating (asterisk) embryos shown. Scale bars: 250 μm.

(**f**) Quantitation of *ap2a1* MO rescue with mouse (*Mm*) α_C-subunit (*Ap2a2*) mRNA.

(**g**-**i**) mRNA expression patterns of Fgf signaling genes in control (g), *ap2a1* (h) or *fcho1* (i) shield- or 30% epiboly-stage morphants. The zones of expanded expression (brackets) are indicated; D, dorsal; V, ventral. Scale bar: 250 μm.

(**j**) Restoration of *dusp6* expression in 30% epiboly (~5 hpf) *ap2a1* MO embryos by coinjection of mouse *Ap2a2* mRNA. Zone of expansion without rescue (brackets) indicated.

(**k**-**m**) Fgf-dependent GFP expression in live embryos injected with 10 ng control, *ap2a1* or *fcho1+fcho2+p53* MOs. Delaminating ectoderm, broadly expanded GFP expression (arrowheads) in *ap2a1*, and diminished ventral tissue (bracket) in *fcho1+2* morphants shown. A, anterior; P, posterior; mhb, mid-hindbrain boundary; r4, rhombomere 4; Kv, Kupfer's vesicle. Elliptical *fcho1* morphant (orange arrow) shown in m. Scale bar: 250 μm.

(**n**-**p**) mRNA expression profiles of early patterning signaling components in control (n), *ap2a1* (o) or *fcho1* (p) shield- or 30% epiboly-stage morphants. Arrowheads and brackets show zones of expanded expression. Scale bar: 250 μm.

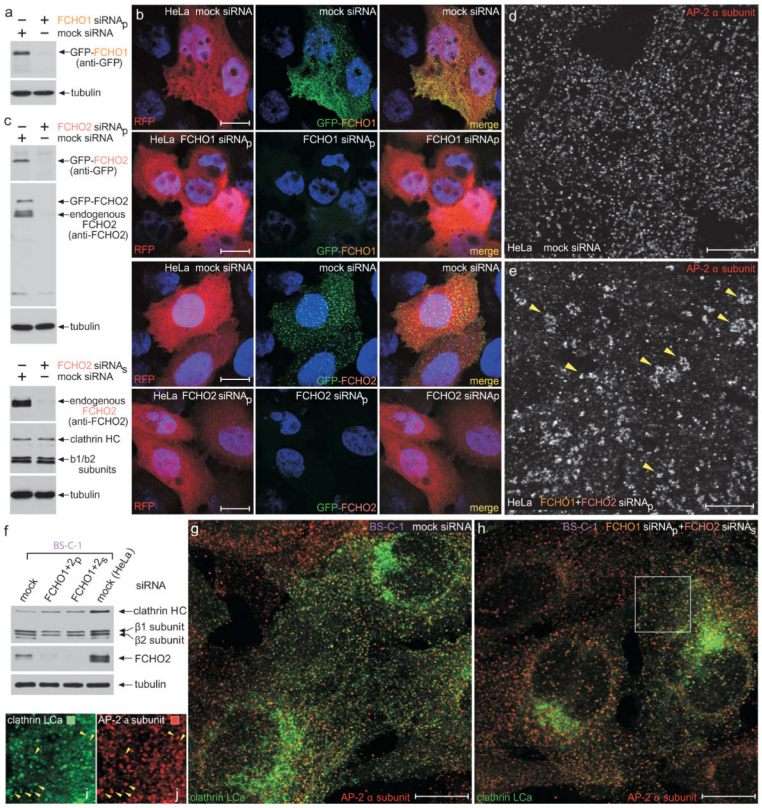

Figure 8.

AP-2–clathrin coats persist in FCHO1 and FCHO2 siRNA-treated HeLa and BS-C-1 cells.

(**a**) Biochemical validation of FCHO1 transcript silencing in GFP-FCHO1-expressing HeLa cells by immunoblot analysis of lysates from mock or FCHO1 siRNA transfected cells. An ON-TARGET plus SMART pool ($siRNA_p$; Dharmacon) was used. Replicate immunoblot with an anti-β tubulin mAb to verify equivalent loading of lysates.

(**b**) HeLa cells subject to mock, FCHO1 or FCHO2 $siRNA_p$ silencing and also ectopically expressing GFP-FCHO1 (along with RFP to mark co-transfected cells) were fixed and stained with Hoechst 33258. Representative, color-separated or merged, confocal optical sections are show. Note that both the FCHO1 and FCHO2 $siRNA_p$ sets efficiently quench the GFP-FCHO1 fluorescence. Scale bar: 10 μm.

(**c**) Biochemical verification of FCHO2 $siRNA_p$- or $siRNA_s$-mediated silencing in HeLa cells by immunoblotting. SDS-PAGE resolved lysates from cells subjected to the indicated treatments were immunoblotted with antibodies against either GFP or FCHO2 and β tubulin as a loading control. Notice that the FCHO2 $siRNA_p$ suppresses both the transfected GFP-FCHO2 as well as the endogenous protein in these cell populations highly efficiently.

(**d-e**) Representative single confocal optical sections of HeLa cells subjected to mock (d) or combined FCHO1+FCHO2 $siRNA_p$ (e) followed by fixation and immunodetection of the endogenous AP-2 α subunit using mAb AP.6. Note that although the roughly regular patterning and surface density of AP-2–clathrin structures is diminished upon knockdown of FCHO1/2, AP-2-positive puncta still persist and, generally appear to increase in size and are more irregularly deposited (arrowheads).

(**f**) Biochemical verification of FCHO1+FCHO2 $siRNA_p$- or $siRNA_s$-mediated silencing in BS-C-1 cells by immunoblotting. Notice, again, that the Stealth (Invitrogen) FCHO2 $siRNA_s$ very effectively extinguishes the endogenous FCHO2 in these populations of cells. Mock transfected HeLa cells included for comparison.

(**g-j**) Representative single confocal optical sections of clathrin LCa-GFP expressing BS-C-1 cells subjected to mock (g) or combined FCHO1 $siRNA_p$+FCHO2 $siRNA_s$ (h) followed by fixation and immunodetection of the endogenous AP-2 α subunit using mAb AP.6. The insets (i, j) show a color-separated enlarged region corresponding to the boxed area in h. Surface AP-2-positive puncta clearly persist in these FCHO1+2-silenced BS-C-1 cells as well (arrowheads). Note that only a subset of clathrin-labeled structures is AP-2 positive in both the mock and FCHO1+2-silenced cells, as clathrin normally assembles on other intracellular structures as well. Scale bar: 10 μm.